INL/CON-13-29950
PREPRINT

Discrete Element Modeling Results of Proppant Rearrangement in the Cooke Conductivity Cell

SPE Hydraulic Fracturing Conference

Earl D. Mattson
Hai Huang
Michael Conway
Lisa O'Connell

February 2014

The INL is a
U.S. Department of Energy
National Laboratory
operated by
Battelle Energy Alliance

SPE 168604-MS

Discrete Element Modeling Results of Proppant Rearrangement in the Cooke Conductivity Cell

Earl D. Mattson, SPE, Hai Huang, Idaho National Laboratory, Michael Conway, SPE, and Lisa O'Connell, SPE, Stim-Labs, Inc.

This paper was prepared for presentation at the SPE Hydraulic Fracturing Technology Conference held in The Woodlands, Texas, USA, 4–6 February 2014.

Abstract

The study of propped fracture conductivity began in earnest with the development of the Cooke cell which later became part of the initial API standard. Subsequent developments included a patented multi-cell design to conduct four tests in a press at the same time. Other modifications have been used by various investigators. Recent studies by the Stim-Lab proppant consortium have indicated that the flow field across a Cooke proppant conductivity testing cell may not be uniform as initially believed which resulted in significantly different conductivity results. Post- test analysis of low temperature metal alloy injections at the termination of proppant testing prior to the release of the applied stress suggest that higher flow fields may be expected along the top of the proppant pack compared to the middle of the pack due to modifications made to the original Cooke cell design. To evaluate these experimental findings, a physics-based two-dimensional (2-D) discrete element model (DEM) was developed and applied to simulate stress distribution in the Cooke cell and proppant rearrangement during conductivity testing as a function of stress. Numerical simulations of the testing apparatus are critical to understanding the impact of modification to the testing cell as well as understanding key proppant conductivity issues.

The 2-D DEM model was constructed to represent a realistic cross-section of the Cooke cell with a distribution of four material properties, three that represent the Cooke cell (steel, sandstone, square rings), and one representing the proppant. In principle, Cooke cell materials can be approximated as assemblies of independent discrete elements (particles) of various sizes and material properties that interact via cohesive interactions, repulsive forces, and frictional forces. The macroscopic behavior can then be modeled as the collective behavior of many interacting discrete elements. This DEM model is particularly suitable for modeling proppant mechanical interactions subjected to an applied stress, where the experimental cell is represented as a cohesive body composed of a large number of discrete elements, and proppants can be modeled as the individual discrete particles with various sizes (following the proppant size distribution-density function used in the test) that exhibit no cohesive strength between the particles.

Initial 2-D DEM modeling results suggest that proppant rearrangement and non-uniform stress distribution can develop across the proppant pack due to square ring modifications. Compaction along the edge of the proppant pack beneath the square ring seal result in a disproportionate lower flow field along these edges as compared to the middle of the proppant pack. These results suggest that reported conductivity values determined by the Cooke cell may be biased to overestimate the actual conductivity of the proppant due to modifications to the standard Cooke cell. Such modifications should be carefully evaluated as to their consequences on determining the proppant conductivity.

Introduction

One of the most important parameters when designing a hydraulic fracturing test is the selection of proppant. Besides the proppant strength, high conductivity of the proppant pack is desirable to maximize production. Most proppant testing is conducted in the Cooke Conductivity Cell (Cook 1975) or some modification of this cell initially following standardized testing described by the American Petroleum Institute (API) Recommended Practices (RP) API RP 61 (API, 1989), and more recently, procedures described by the International Organization of Standardization (ISO) publication ISO 13503-5 "Procedures for Measuring the Long-term Conductivity of Proppants" (Kaufman et al. 2007). The general concept behind the Cooke cell testing is the application of a one- dimensional stress that simulates fracture closure on a proppant pack in the field. The test is run until semi-equilibrium conditions are reached and the proppant conductivity is measured. Then the

stress is increased to a new level and the conductivity test is repeated. Proppant conductivity as a function of the applied stress is typically reported. Proppant suppliers use this information to describe the quality of their proppant product performance under field conditions.

Standardization of test and the testing cell to eliminate testing bias are imperative to compare the expected response of one type of proppant to another. This paper evaluates numerical simulations of the stress distribution within the standard Cooke cell due to a square ring modification for a simulated 20-40 spherical proppant of a known distribution.

Experimental Observations

The ISO 13503-5 standard, "Measuring the Long Term Conductivity of Proppants", established a testing time limit of 50 hours as the time at which the conductivity reaches a semi-steady state value. The ISO procedure also replaced the stainless steel shims with sandstone cores, increased the testing temperature to a value more representative of the reservoir formation, and recommended an oxygen-free silica-saturated testing fluid. Due to some of these modifications from the original API RP 61 procedures, a few practical issues have been noted by laboratory personal.

First, the original Cooke cell often experienced leakage around the square ring seal. Although the square ring was larger than the grove, it was not large enough to ensure a good compression seal between the piston and the wall, especially at low pressures. A simple solution to fix the leakage issue was to increase the size of the square ring in an attempt to increase the contact pressure of the square ring on the cell wall. A rectangular square ring with a cross-sectional dimension of 0.150 inches in width by 0.130 inches in depth was one attempted solution. However, the square ring groove cross-sectional dimension is smaller than the square ring (dimensions of 0.123 inches in width by 0.122 inches in depth) causing large deformation of the square ring during placement (Figure 1a) in the Cooke cell.

In addition, tolerances in the original API design were too tight to allow free piston movement within the cell. Machinists building the cell recognized this issue and have reduced the piston width slightly to allow free movement. However, the solution to the leakage issue and the undersized pistons caused extrusion of the square ring beyond the piston face. Post-testing experimental observations (Conway and O'Connell, 2013) indicate that during testing the Viton square ring is partially extruded into gap areas between the piston and the Cooke cell wall, the stainless steel shim and the Cooke cell wall, as well as the stainless steel piston and the stainless steel shim (Figure 1b). At fluid pressures greater than 1000 psi, the manufacturer recommends that gaps should be no more than 0.010 inches (EMP seal handbook) for O-ring materials with a durometer of 70. The load pressures applied to the Cooke cell are sufficient to cause extrusion issues along the piston wall and beneath the piston. The square ring deformation causes bridging of the piston to the stainless steel shim and sandstone core along the outer circumference of the testing surface.

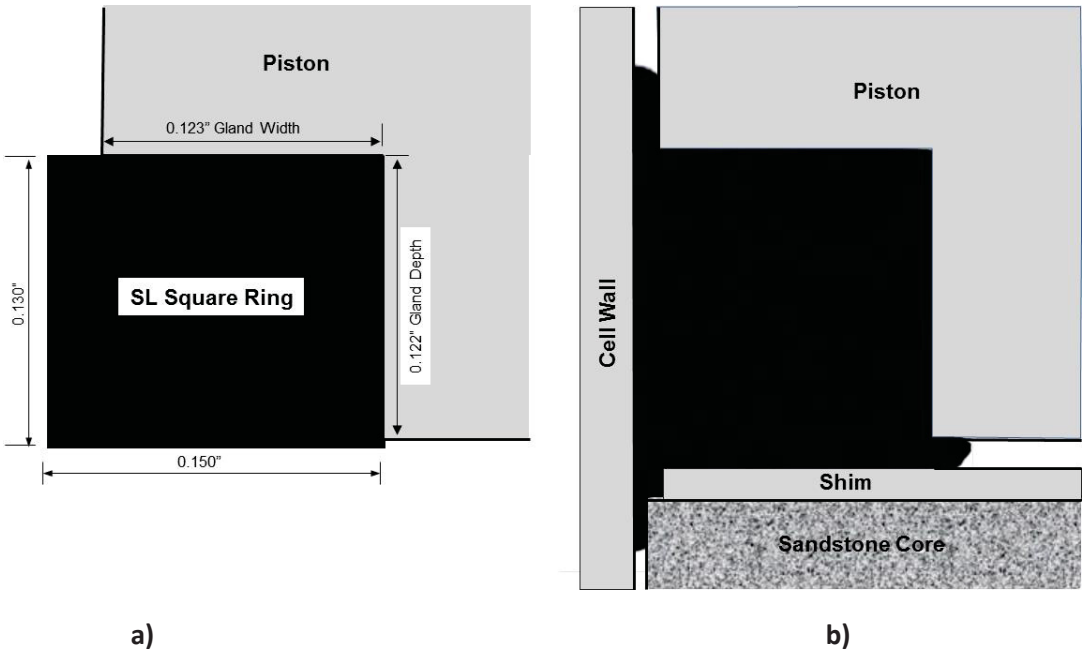

Figure 1. Viton square ring in a Cooke cell, a) cross section of initial insertion of the Viton square ring in the upper piston, b) extrusion of the Viton square ring into gaps.

With rectangular square rings, the extrusion of the Viton into the gap between the piston and the shim in the standard Cooke cell may cause stress concentration along the outer edges of the testing area. Figure 2a illustrates the location of stress concentration at the outer edges of the shim and sandstone core due to the oversized square ring. Figure 2b supports this hypothesis through the observation of post-test deformation of the stainless steel shim towards the sandstone core. Further evidence of stress concentration due to this square ring design was obtained by examining the sandstone core and flow pathways in the proppant pack. Figure 3a is a photograph of a tensile crack formation down the center of the sandstone likely due to stress concentration along the edges of the test cell. Unlike the stainless steel shim, sandstone has low tensile strength and cannot support non-uniform stresses without failure.

Alloy 117 was injected into the proppant pack at the end of the test to examine the conductivity flow pathway distribution at the end of testing but prior to the removal of the final stress. Alloy 117 is a metal that is liquid above 117^{o}F but is a solid at room temperatures. As the alloy hardens, it preserves the porosity distribution of the proppant pack for post-test analyses. Figure 3b illustrates that the liquid metal was able to be injected through the entire proppant surface. The surface of the proppant pack did not indicate bulging of the middle of the proppant pack with the exception of a small preferential pathway (Figure 3c) associated beneath the crack in the sandstone core at the sandstone/proppant interface. Although the sandstone core fractured, no metal was found in the sandstone core fracture itself, suggesting that there was no preferential flow through the sandstone core.

Although modifications to the square ring of the Cooke cell appear to be minor, the rectangular square ring may cause a bias in the measured proppant conductivity values. Figure 4 illustrates conductivity as a function of time for eight tests under a 2000 psi load using identical proppant for all tests. Four tests were conductivity in a standard groove (SG cell data) with rectangular square rings (Figure 2a) whereas the other four tests (DG cell data) were conducted in a modified Cooke cell with deeper square ring grooves (Figure 2b) that were more properly designed to accommodate the rectangular square ring.

Proppant conductivity results suggest that all 4 of the SG cell proppant conductivity measurements are larger than those tested using the DC cells. On average, the SG cells had a conductivity value approximately 50% higher than that of the modified deep groove designs.

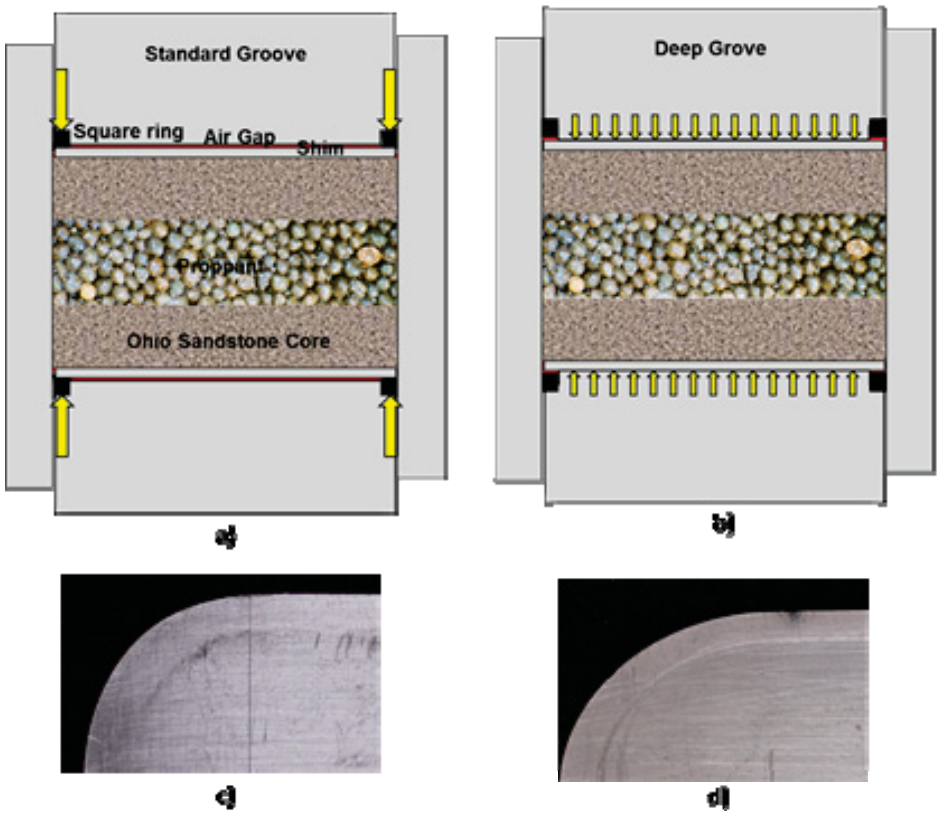

Figure 2. Cross- section of a) the Standard Cooke cell with under-sized square ring groove. Yellow arrow s represent stress concentration, red shading represents air gap, b) redesigned deep groove Cooke cell. Post-test photographs of stainless steel shims; c) shim deformed away from square ring, and d) shim deformed towards square ring (modified from Conway and O'Connell, 2013).

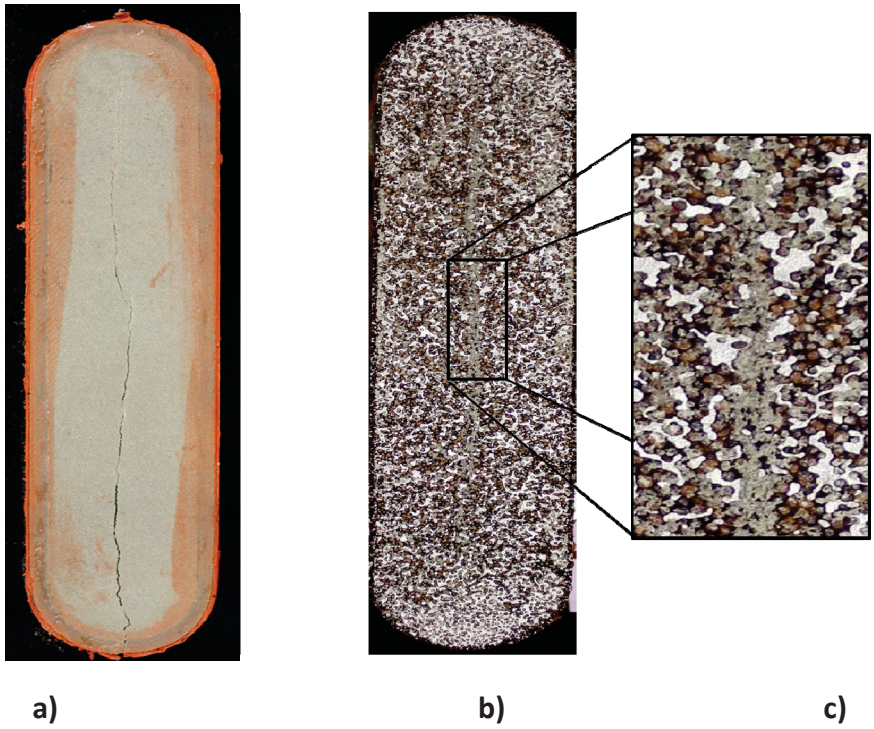

Figure 3. Post-test observations of a) the sandstone core with tensile crack, b) view of proppant surface that has been stabilized with Alloy 117 metal injection, and c) close up of stabilized proppant illustrating slight preferential flow pathway along crack (from Conway and O'Connell, 2013).

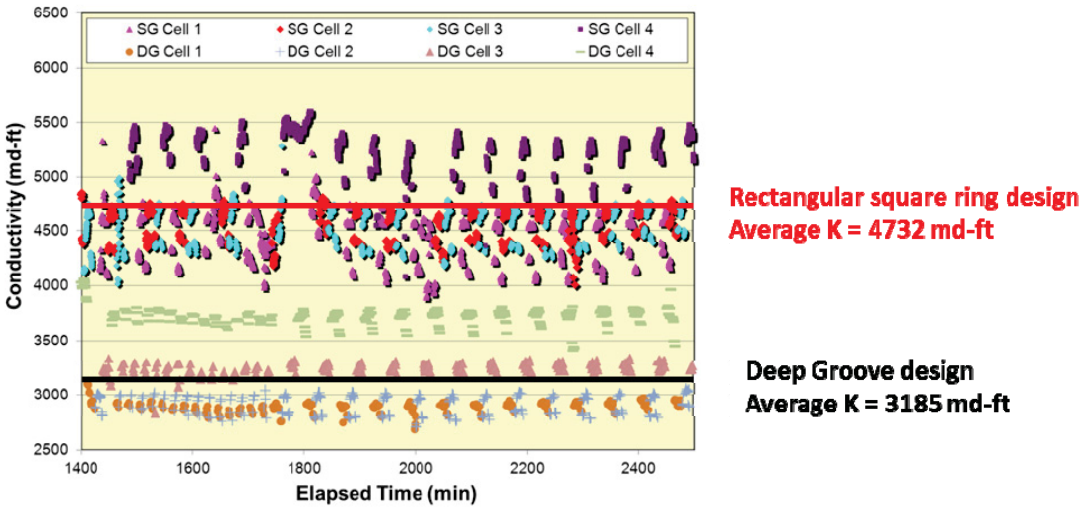

Figure 4. Comparison of calculated proppant conductivity using two Cooke cell designs; the rectangular square ring in a Cooke cell (SG cell data, red) and a modified Cooke cell with deep grooves (DB cell data, black) (from Conway and O'Connell, 2013).

Model

To better understand these experimental observations, and to help evaluate other modifications to the Cooke cell, a discrete element method (DEM) model was constructed to examine the geomechnical behavior within a standard Cooke cell during a long-term proppant conductivity test. DEM was chosen as to its ability to simulate the dynamic movement of the proppant particles and Viton square ring during the application of stress as well as generation of the crack in the sandstone core.

The DEM model originally introduced by Cundall and Strack (1979) over 30 years ago, has been widely used by the geotechnical engineering community to model the mechanical deformation and fracturing of polycrystalline rocks at various scales, ranging from grain-scale microcracks to large-scale faults associated with earthquakes (Cundall, 2001). In DEM models, a volume of material is represented by a network of nodes (also referred as particles) of variable sizes connected by mechanical elements that can be a variety of rheo-mechanical properties, depending on the application. In this work, the nodes were connected by elastic beams.

For isotropic elastic media, two independent elastic constants, the Young's modulus, E_o, and shear modulus, G_o, are commonly used to describe the media mechanical properties. If a random DEM network was used to avoid the effects of lattice symmetry on the fracturing pattern and represent the small scale heterogeneities that are present in all materials, constants in the model must be calibrated against the desired values of E_o and the Poisson ratio. At mechanical equilibrium, the total force and moment acting on every DEM node must vanish, giving rise to the Cosserat elasticity equations in the continuum limit.

A 2-D model domain with approximately 15,000 particles was used to simulate tests in the Cooke cell. Only the top half of the Cooke cell was simulated since there would be stress symmetry along the midpoint of the proppant pack as illustrated in Figure 5. General dimensions of the simulation boundary are 1.5 inches wide, with material heights of ; proppant (0.12 inches), sandstone (0.35 inches), stainless steel shim (0.06 inches), air gap (0.039 inches), and stainless steel piston (~0.3 inches). The air gap was estimated by conservation of area of the square ring groove and the rectangular piston. Boundary conditions were established as no horizontal movement along the side walls and no downward movement at the midpoint of the proppant pack. Four different materials (stainless steel, Ohio sandstone, Viton rubber and 20-40 proppants) were used in these simulations. Each of these materials was assigned a different critical longitudinal tensile strength to describe the particle-to-article adhesion. Stainless steel has the largest critical longitudinal tensile strength values while proppant has a value near zero to represent a non-cemented porous media. For fracture initiation and growth in the sandstone core, the beam between two particles was removed if it fails to satisfy the von Mises Failure Criterion.

Proppant was represented by selecting particles of a range of diameters that simulate a 20-40 proppant pack. For these simulations, we chose a normal distribution of particle diameters passing a 20-mesh sieve and retained on a 40-mesh sieve. These particles were randomly placed in the Cooke cell and allowed to slightly settle to represent the filling of the Cooke cell with a real proppant. A smaller uniform particle size to represent the isotropic homogeneous behavior for the sandstone, rubber and stainless steel materials.

Stress was applied by imposing a slight downward vertical displacement of the upper stainless steel particles (shown as Δx in Figure 5b) and allowing the model to adjust to this strain displacement. Due to the large Young's modulus of stainless steel, this displacement will quickly transfer to materials that have a lower Young's modulus. Once a mechanical load is applied, an over-relaxation algorithm was used to relax the DEM network to a new state of mechanical equilibrium in which the net forces and moments are zero for all DEM particles. The spatial distribution of the resulting stress-strain fields were calculated and plotted to better understand the interactions between of the different materials.

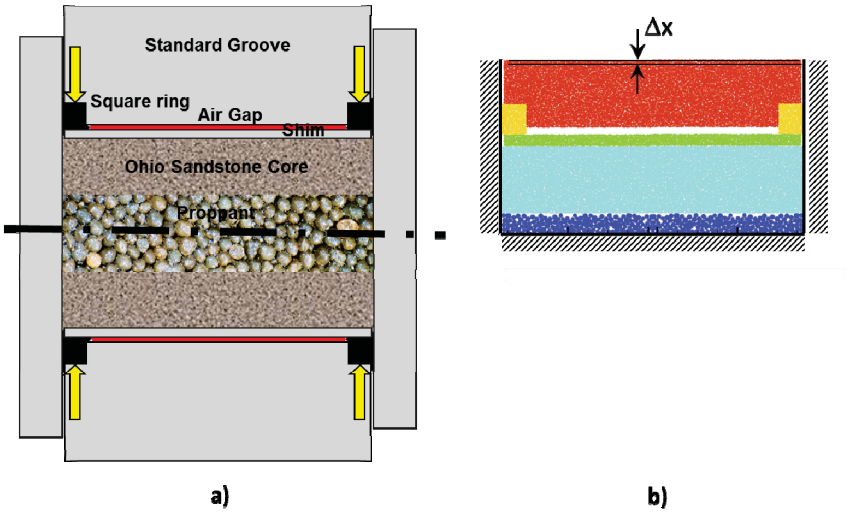

Figure 5. Conceptual cross-section of a) standard Cooke cell and b) DEM model cross-section used in simulations. R red is stainless steel, yellow is Viton rubber, white is the air gap, green is stainless steel, light blue is sandstone, and dark blue is the proppant.

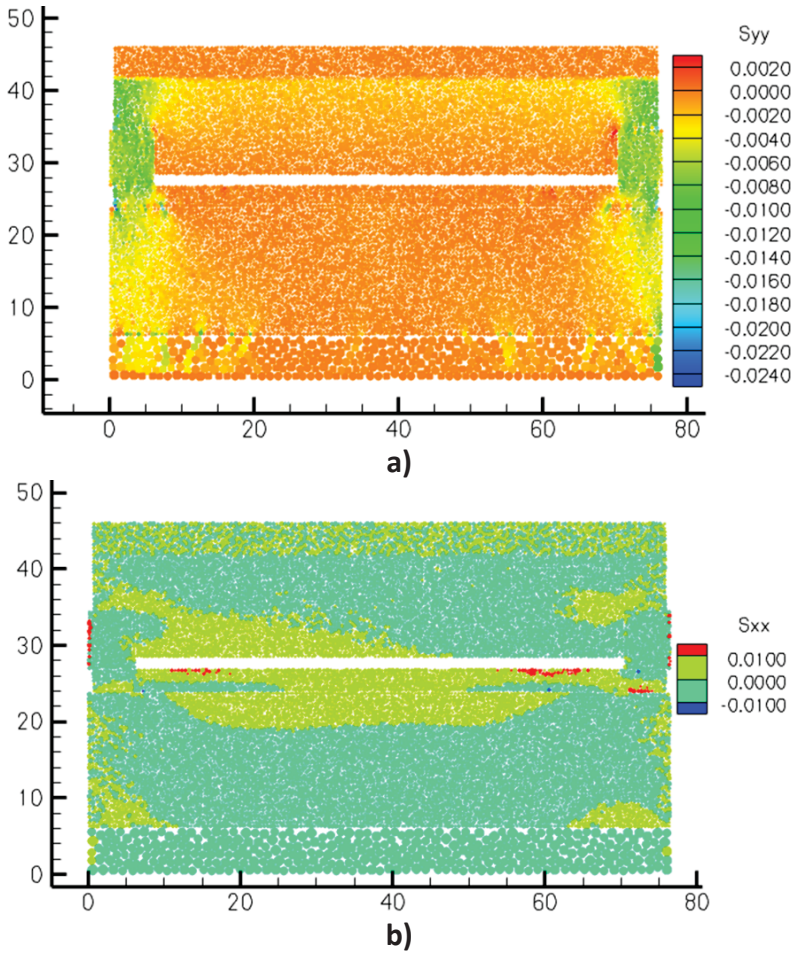

Figure 6. DEM 2-D modeling simulation results of the stress distribution in the standard Cooke cell with rectangular square rings; a) the vertical stress field (green and yellow represent high vertical stress locations), b) the horizontal stress field (yellow and red represent zones of tension).

Model Results

DEM model simulations were conducted to examine the expected stress distribution and proppant rearrangement within the Cooke cell. The total vertical uniform displacement of the upper surface of the piston was limited to 2% of the total height. As an initial evaluation of the stress distribution, relative Young's moduli were assigned to the four materials (stainless steel 100, proppant 3, sandstone 1, Viton 0.1) and the stress was also output in dimensionless units. Figure 6 illustrates the vertical (Syy) and the horizontal (Sxx) stress fields for the standard Cooke cell with rectangular square rings at the termination of the simulation. Since the model was built with dimensionless parameters, the x- and y-axis are also dimensionless.

Figure 6a illustrates the vertical stress for the DEM particles. Orange colored particles illustrate zones of near zero vertical stress whereas the cooler colors depict zones of large compressional vertical stress. The darker orange zone along the upper surface of the stainless steel piston is the location where the uniform downward displacement was implemented. The uniform strain just underneath this upper boundary quickly dissipates and illustrates a concentration of the vertical stain through the rubber square rings. However, unlike that the stainless steel piston above the air gap, the stainless steel shim and sandstone materials do not evenly redistribute the vertical stress to the proppant pack. The proppants immediately below the square rings exhibit the largest vertical stress field. The proppants in the middle of the Cooke cell have almost no vertical stress.

Horizontal stress for the Cooke cell is shown in Figure 6b at the end of the simulation. For this case, the zone used to apply the stress shows a mixture of positive (green particles) and negative (blue particles) horizontal stress due to the applied displacement. The stainless steel piston is mostly in horizontal compression with a zone of tension (green particles) just above the air gap. More interestingly, the stainless steel shim is in tension beneath the air gap as is the upper portion of the middle of the sandstone core. Proppant due to its ability to be repositioned exhibits little horizontal stress.

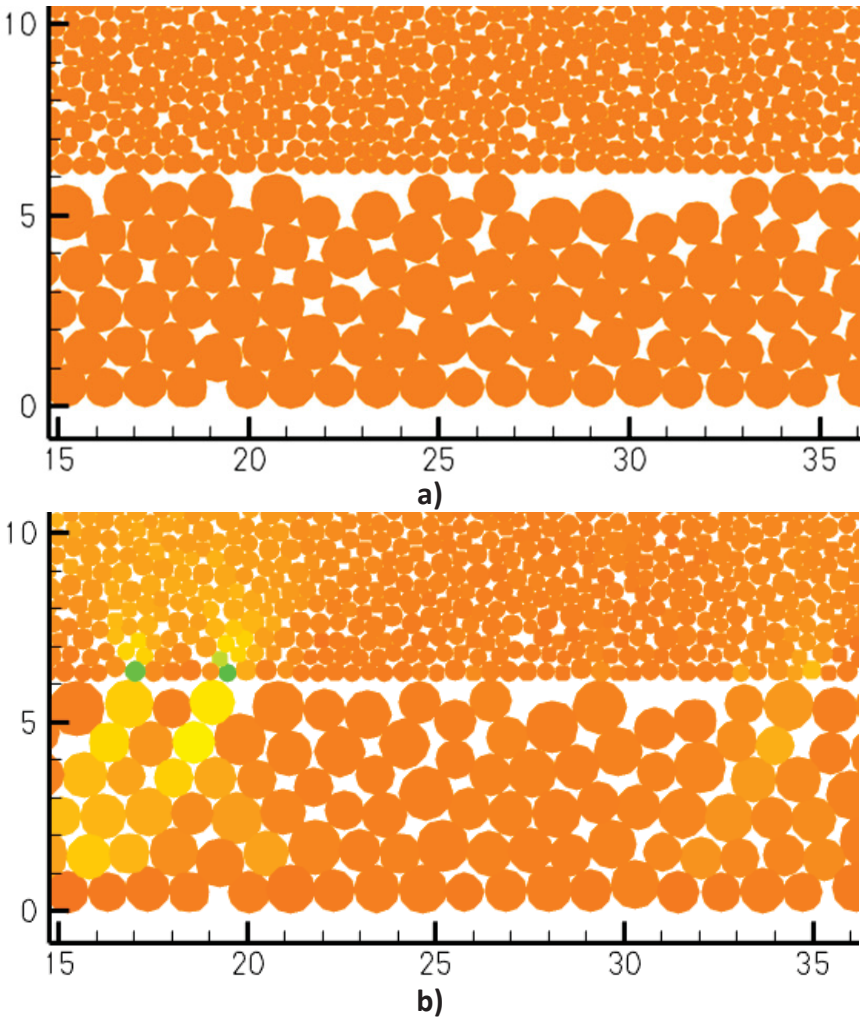

Figure 7. Close up of the overlying sandstone core and proppant pack illustrating the rearrangement of the individual proppants; a) initially proppant pack prior to the application of piston displacement, b) final proppant location after compaction and proppant rearrangement. Proppant color represents the vertical stress of the individual proppants. Orange is zero vertical stress; green represents locations of proppant/sandstone interaction induced stress.

The shape of the horizontal tension on the stainless steel shim and sandstone core indicate a potential upward bending of these materials with rectangular square rings and the presence of an air gap. Although the calculated horizontal tension in the sandstone was not sufficient to break any proppant bonds (with the material parameter and overall piston displacement) the zone of tension is in agreement with the fracturing of the sandstone cores as illustrated in Figure 3a.

Proppant position in the standard Cooke cell is illustrated in Figure 7. Figure 7a show a close-up of the proppant particles and the lower portion of the sandstone towards the middle of the Cooke cell prior to vertically displacing the stainless steel piston. In these figure, the orange color represents zero vertical stress whereas colder colors represent vertical compression on a particle. When the proppants are placed in the cell, a nearly uniform layer develops on the lower no vertical displacement boundary whereas the top surface of the proppant pack is only partially filled. After the piston is depressed, Figure 7b, the proppant particles are displaced to fill the additional void space at the top of the proppant pack. This may be best seen by examining the upper proppant locations relative to the sandstone core at horizontal locations 23 and 29 in Figure 7a and b. Also interesting in Figure 7b, is the fact that not much of the proppant pack in the middle of the standard Cooke cell is supporting the applied stress. Only at locations with proppant-sandstone contacts is a compressional stresses noted in the sandstone and transferred to the underlying proppant particles.

Displacement vectors were plotted for the DEM particles in Figure 8a and 8b. The arrows show the direction of movement of each particle from its original position and the length of the arrow is an indication of the displacement magnitude. The particle colors also indicate the magnitude of a particle's vertical displacement. Cold colors are large vertical displacements in the downward direction whereas warmer colors represent vertical displacement in the upward direction. The stainless steel piston has the most vertical downward displacement as it fills the air gap and compacts the rubber square

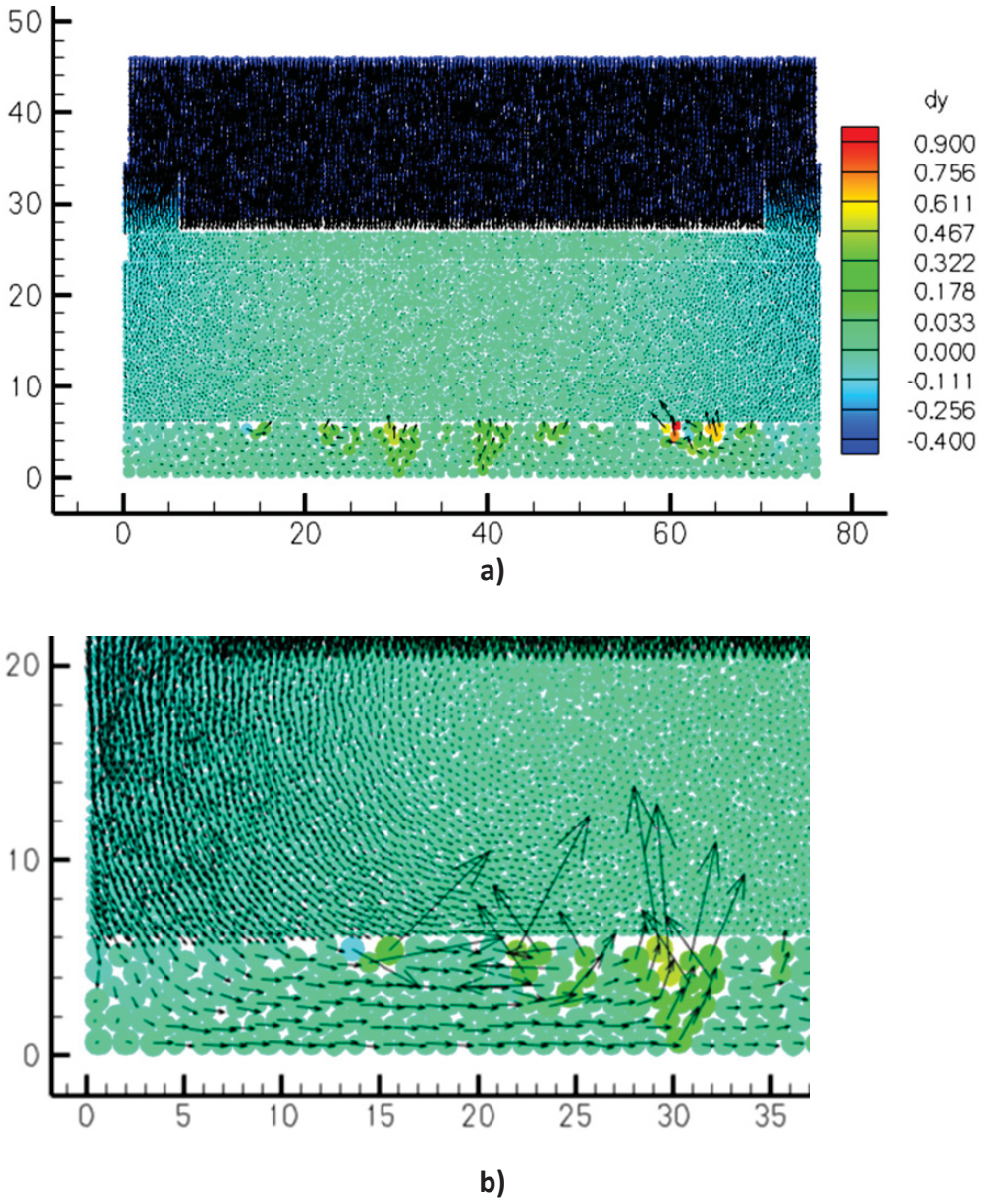

Figure 8. DEM particle displacement field vectors indicating direction of magnitude of particle movement relative to the stainless steel piston displacement. a) total DEM domain, and b) close up of lower left-hand corner. Particle color represents vertical displacement.

ring. The stainless steel shim, sandstone core, and proppant move downward along the outer walls of the Cooke cell and upward through the middle of the Cooke cell. The largest upward movement is noted for proppants near the sandstone-proppant interface. Figure 8b is a closer examination of the lower left-hand corner showing a shift of the proppants from the Cooke cell edge towards the center of the cell.

Summary

Modifications to the Cooke testing cell have the potential to bias long-term proppant conduct ivy testing results.
Experimental testing results suggest that even small changes to the square ring seal have been noted to have the ability to bias laboratory testing results by 50%.

A 2-D DEM model was developed to evaluate the stress distribution within the Cooke cell during testing. Model simulation results suggest that due to the over-sized square rings and resulting air gap between the stainless steel piston and the stainless steel shim, the resulting stress from the applied load is concentrated through the square rings onto the stainless steel shim and sandstone. The shim and the sandstone are not strong enough to redistribute the stress evenly across the

sandstone-proppant interface to the proppant. As a result, a slight bowing of the shim and sandstone occur that causes the proppant to be rearranged towards the center of the Cooke cell as well as upwards in the middle of the proppant pack. Simulation results are consistent with laboratory experimental observations of shim deformation and sandstone core fracturing.

These preliminary modeling results, although not fully calibrated to the material properties, support the hypothesis that the rectangular square ring modification to the standard Cooke cell resulted in a non-uniform stress field across the proppant pack and a rearrangement of the proppants toward the middle of the proppant pack. Additional modeling will be conducted to examine the subsequent deep groove modification to fix to the rectangular square rings in the standard groove Cooke cell as well as to evaluate an algorithm to determine the proppant porosity spatial distribution.

In addition to developing standardized proppant conductivity testing procedures used to evaluate the quality of proppant materials (e.g. API, ISO), test cell apparatus standardization is also needed to ensure consistent conductivity results for proppant testing. Modeling standardized test cells and any subsequent modifications to these cells would ensure the proppant conductivity testing is being performed as designed.

Acknowledgements

The authors would like to thank the Stim-Lab Proppant Consortium for sharing experimental observations of the proppant conductivity testing results and the Idaho National Laboratory's Laboratory Directed Research and Development program, project 13-114.

References

API RP 61, 1989. Recommended Practices for Evaluating Short-term Proppant-Pack Conductivity, first edition, Washington, DC; API.

Conway, M.W., and L. O'Connell, 2013, 4.2 – Conductivity Variations between Piston Designs, presented at the Stim-Lab Proppant Consortium Meeting, Rohnert Park, CA, July 18-19, 2013.

Cooke Jr., C.E. 1975. Effect of Fracturing Fluids on Fracture Conductivity. J. Pet. Technol. 27 (10): 1273-1282. SPE-5114-PA.doi: 10.2118/5114-PA.

Cundall, P.A. and O.D.L. Strack (1979), Discrete numerical-model for granular assemblies, Geotechnique, 1979. 29(1): p. 47-65.

Cundall, P. A. (2001), A discontinuous future for numerical modelling in geomechanics?, Proc. Inst. Civil Eng.-Geotech. Eng., 149(1), 41-47.

EMP Seal Handbook, The Seal man's O-Ring Handbook, pg. 112, http://www.thesealman.com/pages/oring_handbook/pdf_files/epm_oring_hbpt4.pdf

Kaufman, P.B., R.W. Anderson, M. Ziegler, A.R. Neves, M.A. Parker, K. Abney, G.Warwick Kerr de Paiva Cortes, S. Joyce, and G.S. Penny. Introducing New API/ISO Procedures for Proppant Testing, SPE 110697, 2007 SPE Annual Technical Conference and Exhibition held in Anaheim, California, U.S.A., 11–14 November 2007.